Journal of the Chinese Chemical Society, **1994**, *41*, 335-343

Invited Paper

Classical Cascade Calculations on the Analysis of Surface Bonding Structures by Secondary Particle Mass Spectrometry

Che-Chen Chang (張哲政)
Department of Chemistry, National Taiwan University, Taipei, Taiwan, R.O.C.

The application of secondary particle mass spectrometry to analyze the atomic bonding configuration on a surface was investigated with computer calculations of particle sputtering from an Ar-bombarded surface of Ag{111}. In contrast to the prediction from the present sputtering theory, better resolved structure in the angular distribution was not observed for particles of high energy sputtered from the surface. These particles ejected to a wide angle and their angular distribution may not reflect well the atomic bonding geometry on the surface. The analytical capability of secondary particle mass spectrometry to determine surface structures can be significantly improved by selecting for detection only those particles that have prolonged collisions. The preferred directions of ejection and the relative sputtering intensity in the distribution of azimuthal angle between major open channels on the surface vary insignificantly with the duration of collision in the regime of long collisions. The results provide the first evidence that at small energies of sputtering the particles emitted from the surface may contain information about only the top two surface layers. Secondary particle mass spectrometry can thus be extremely surface sensitive for analysis of properties of solid surfaces.

INTRODUCTION

Interest in analysis of solid surfaces increased rapidly during the past two decades at the demand of miniaturization of optoelectronic devices.[1,2] The interest reflects that knowledge of exact substrate composition and the capability to control surface properties are prerequisite to further development of nanotechnology. The role of the surface becomes more critical as the physical dimension of the materials approaches the nanometer scale. The continued development of surface techniques to analyze precisely surface properties and to characterize accurately chemical reactions occurring on surfaces is thus essential for production of high-performance devices with desired chemical stability.

Analysis of the geometry of atomic bonding at the surface represents a unique approach to understand chemical reactions on surfaces. Among techniques[3] used to analyze this geometry, secondary particle mass spectrometry[4,5] is particularly powerful because of its high detection sensitivity. Early work[6] showed that the angular anisotropy of atoms sputtered from single crystals reflected the atomic bonding symmetry of the target crystal face. This observation was significantly extended in detailed investigation of fundamental processes of sputtering, and theories to utilize the technique to elucidate the reaction chemistry and the geometric structure of clean and adsorbate-covered surfaces were developed.[7-12] With a molecular dynamical model to simulate sputtering, various Wehner-type spot patterns were reproduced in calculations of various crystal surfaces. These spot patterns clearly showed that the ejection direction of the sputtered species was greatly influenced by the atomic bonding geometry on the surface. Tracing individual atomic trajectories revealed that there was a surface channeling mechanism that governed the behavior of the ejecting species. According to this mechanism, the ejecting particles moved preferentially along open crystallographic directions on the surface. This surface channeling effect was more influential to the path of sputtered species that ejected with large kinetic energies (> 20 eV) than that with small energies. The latter species were believed to eject late in the collision cascade when the initial surface order was destroyed.[7] Further, in the case in which ionic sputtered species were detected, the trajectory of highly energetic ionic species was closer to that of neutral atoms than the trajectory of weakly energetic species. The presence of the image force caused the ions of 20 eV to deflect by less than 2° closer to the surface.[7] Surface atomic bonding structures may thus be deduced from the angular distribution of the sputtered energetic species using secondary particle mass spectrometry.[8,11,13-15]

This sputtering theory for analysis of atomic bonding geometries on surfaces was developed mostly based on results of computer calculations made on small model crystallites and with a few hundred trajectories. The computations

were protracted, as the events initiated in the surface by particles striking the sample were complicated. However, we found in early work[16] exceptions to the present sputtering theory about the dependence of the angular distribution on the detection condition. A thorough examination of the existing theory is timely, as computational capability improved greatly during the past decade.

Here we report results of full molecular dynamical calculations of Ar bombardment on the Ag{111} surface. The incident energy in the calculation was chosen to be 2 keV, which is an impinging energy commonly used in experiments on static secondary particle surface analysis. This energy is greater than those used before to develop the present sputtering theory. It is expected that the required duration of computation is also increased accordingly, because the momentum of more energetic incident particles tends to dissipate within a larger crystal. The size of the model crystallite used in the calculation was also increased significantly so as to include all sputtering events in the simulation. Finally, for improved statistical accuracy, the number of impact points calculated in this work was also increased substantially.

THE CALCULATION

The mechanistic details of the sputtering process that takes place due to particle bombardment were predicted using classical dynamics.[17] The basic computational scheme is reported in detail elsewhere.[17,18] In this scheme, the motion of all surface atoms plus the bombarding particle was developed in time by integrating Hamilton's equations of motion. The interaction potential functions between the colliding partners were assumed to be additive pairwise. To describe the interaction between the incident Ar particle and the surface Ag atom, the Moliere approximation to the Thomas-Fermi potential was used with the screening length calculated following the Firsov model.[19] The interaction between the substrate atoms was assumed to be a Morse-Moliere splined potential.[20]

To enhance the computation efficiency, a moving atom approximation was employed in this work to simulate the development of the collision cascade in solids. In this approximation, a group of possible interaction partners in the substrate is first determined for each moving particle based on the interaction potential between the moving particle and its possible partner. A largest potential function range about 1.2 times the lattice parameter was used in the calculation to determine the number of interaction partners in the group. The subsequent motion of the particle was then decided by considering the force exerted on it by its interaction partners. Only the equations of motion for the moving particles were integrated. The group of interaction partners of each moving particle was updated every several timesteps.

The model crystallite of the sample target was constructed by placing the substrate atoms at the corresponding lattice sites. The size of the crystallite used for the simulation is about 5 nm by 5 nm, with a thickness of six atomic layers. This sample size was sufficiently large to contain almost all sputtering processes for all impacts. The structure of the microcrystallite was uncorrected for the surface selvage effect.[21]

The simulations were made on DEC Vax 8550 and 3400 computers, with the Ar atom impinging normal to the surface. Impact points over a small irreducible area near the center of the surface were selected for calculation. This area, with an elementary symmetry corresponding to the incident condition and the surface of the specified configuration, was chosen to be a triangle with a size one sixth of the primitive cell. In total 1840 impact points were then allowed to be uniformly distributed within the chosen area.

For each collision sequence that resulted in sputtering from the surface, the initial conditions as well as the collision durations, final energies, and final angles of the ejected particles were stored for subsequent analysis. The collision cascades that resulted in ejection to selected angles of interest and with selected kinetic energies were recalculated in order to examine in detail the related sputtering process. To perceive better the mechanistic details of the sputtering process induced by collision, the ejection mechanisms that resulted in maximum intensities in the angular distribution were analyzed by sketching atom-motion pictures. The picture depicts in time the sequence of three-dimensional atomic displacement for all substrate atoms around the target.

RESULTS AND DISCUSSION

Fig. 1 shows the calculated sputtering yield for Ag particles ejected from the surface due to Ar atom bombardment. The yield distribution shows that the size of the model crystallite chosen for this test is adequate, as only about 2% of the particles were sputtered from the crystalline edges of a thickness of two atomic layers. The sputtering yield decreased rapidly for a substrate atom located farther from the impact zone (the dark triangle in Fig. 1). About half the sputtered particles originated from atoms initially residing within two lattice spacings of the target atom. More than three quarters of the sputtered species were from substrate

atoms located within three lattice spacings from the target. The ratio of the number of sputtered particles originating from atoms located at distances more than four lattice spacings from the target to the total number of the sputtered particles was less than 0.08. The sputtering process is thus quite localized and secondary particle mass spectrometry operated in the static mode can thus be used to analyze the characteristics and the bonding geometries of solid surfaces. The results also indicate that, for a rapid and qualitative description of the process of particle emission induced by a collision, computer simulations with a model crystallite smaller than that we used may be performed.

Fig. 1 shows that most particles sputtered from the surface originated from the top two atomic layers. Approximately 95% of the atoms ejected from the top layer of the substrate, compared with ~91% for particles sputtered from the Ag{100} surface[22] and ~76% for those sputtered from Ag{110}.[23] The other 5% of sputtered particles were almost all from the second layer of Ag{111}, compared with ~8% for particles sputtered from the second layer of the Ag{100} surface[22] and ~21% for particles from Ag{110}.[23] The total sputtering yield per incident atom, S, is a function of the crystal orientation, with the yield ratio about 3 : 2 : 1 for $S_{\{111\}} : S_{\{100\}} : S_{\{110\}}$. The observed variation of the relative sputtering yields of these three faces may be qualitatively explained according to transparency theories[24] of sputtering. If the surface atomic density is large the momentum from the incident atoms is retained near the surface. The structural damage at the surface created by bombardment of an energetic particle is thus retained nearer the surface when the {111} face of the face-centered cubic crystal is exposed to the incident beam than when the {110} face is exposed.[25] The open face allows incident atoms to penetrate through holes in the surface and to move deeply into the substrate. The energy of the incident particle is thus deposited in the bulk of the solid and ejection of particles may occur from deeper layers. The total yield per incident atom is thus small for sputtering from the open surface and the structural damage on surfaces of this type is small. The rapidly decreasing sputtering yield from all these surfaces for atoms residing at increasing depth reveals that information obtained from emission of atoms due to particle bombardment is specific to the surface.

The development of sputtering theory generally involves also the characterization of the distribution of kinetic

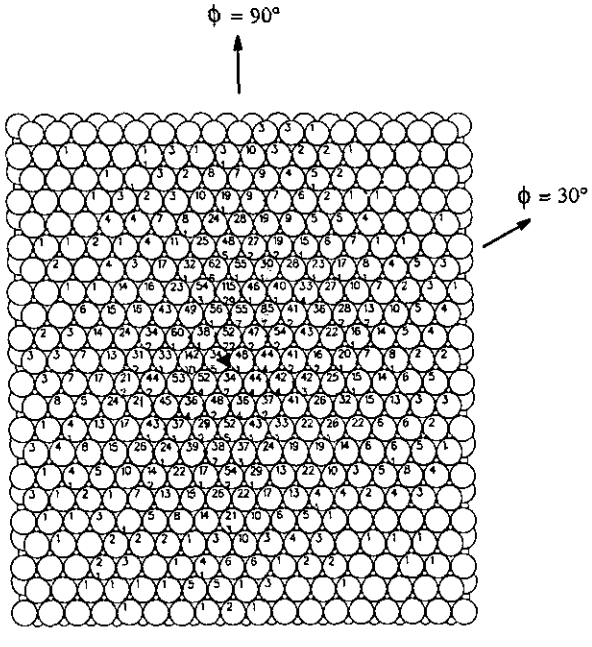

Fig. 1. Percentage of time Ag ejects when averaged over 1840 impact points selected in the triangular zone shown in the center of the crystallite. If two numbers are given, the upper one applies to the first-layer atom and the lower one to the second-layer atom. The number between two atoms aligned horizontally is for an atom in the third layer. Particles are ejected due to bombardment of silver by Ar atoms of energy 2 keV at normal incidence. The horizontal direction corresponds to the <110> azimuth.

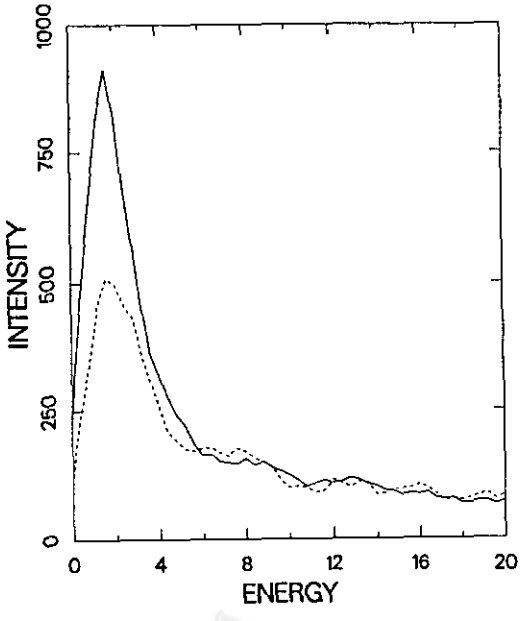

Fig. 2. Distribution of energy (in eV) of particles ejected in directions along ϕ = 30° (dashed curve) and ϕ = 90° (solid curve), respectively, from the Ag{111} surface under bombardment by normally incident Ar atoms with energy 2 keV.

energy of sputtered particles.[26-30] The calculated distribution of energy of particles sputtered from the Ag{111} surface is shown in Fig. 2. This distribution has a maximum about 2 eV for particles sputtered along the direction with either $\phi = 30^\circ$ or $\phi = 90^\circ$. The energetic tail extends to more than 500 eV in both directions. The distribution in the energy regime of more than the most probable ejection energy decays as

$$Y(E) = \frac{CE}{(E + E_b)^n}$$

in which E is the ejection energy, Y the number of ejected particles having kinetic energy E, E_b the surface binding energy of the ejecting particles, and C a collection of constants.[31,32] The exponent n is ~1.8 for sputtering along the direction with $\phi = 30^\circ$ and ~2.2 for sputtering along that with $\phi = 90^\circ$. The spacial distribution of species ejected from an impulse of incident particles may thus be estimated from their approximate kinetic energy distribution. The energy distributions shown in Fig. 2 are much different from that expected for the process of thermal evaporation according to a Maxwell-Boltzman distribution and the width is considerably smaller. The sputtering of particles from this system thus may not result from the thermal spike process.[33]

In the ejection regime of energy more than 6 eV the yield of all particles sputtered along the direction with $\phi = 30^\circ$ is about equal to that along the direction with $\phi = 90^\circ$. According to the present sputtering theory,[7] the path of ejecting particles is constrained by atoms nearby. The sputtered particles thus proceed along the open channel between the nearby atoms on the surface and their angular distribution reflects well the atomic bonding geometry on the surface. Because of the presence of the second-layer atom, the channel in the direction with $\phi = 30^\circ$ is less open than the one in the direction with $\phi = 90^\circ$. Hence the sputtering yield along the direction with $\phi = 30^\circ$ is smaller than that along the direction with $\phi = 90^\circ$. The difference of sputtering yields along these two major channels is expected to be large for energetic particles sputtered from the surface. According to the sputtering theory, these energetic particles eject early in the cascade when much surface order is still retained and when the open channel remains undisrupted.[7] The theory thus predicts that the sputtering yield between the one along the azimuth with $\phi = 90^\circ$ relative to that along $\phi = 30^\circ$ is increased for particles ejected with greater kinetic energy. The results shown in Fig. 2 agree poorly with the prediction based on this theory. The results shown in Fig. 2 indicate that a direct analysis of the surface bonding geometry based on this theory may be inapplicable in some systems.

Further calculations were made to understand the sputtering behavior of particles ejected along these two azimuths. Results from calculations of the distributions of azimuthal angle at various kinetic energies, in the range 0 - 16 eV, appear in Fig. 3. Only those Ag atoms sputtered with a polar angle of ejection 45° from the surface are exhibited in the figure. A polar angle 45° was selected because many static secondary particle mass spectrometric measurements are made at this angle. This figure shows that the distribution is sensitive to variations in the kinetic energy of ejection. At small energies (0 - 1 eV), the sputtering intensity peaks in the directions with $\phi = 90^\circ$, -30°, and -150° (the $<\bar{2}11>$ azimuths). Minimum sputtering intensities were observed about the directions with $\phi = 150^\circ$, 30°, and -90° (the $<2\bar{1}\bar{1}>$ azimuths) for particles sputtered in this energy regime. The large variation of sputtering intensities along the two <211> azimuths indicates that the ejection behavior at

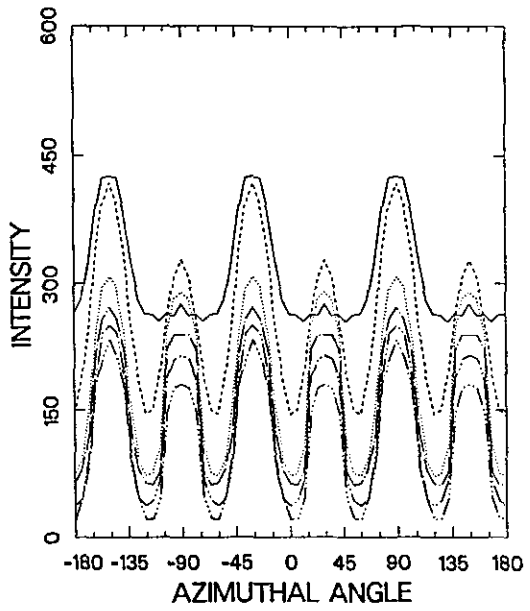

Fig. 3. Calculated distributions of azimuthal angle (in degree) at the polar angle of detection 45 ± 7° for particles sputtered from a Ag{111} surface bombarded by Ar atoms of energy 2 keV at normal incidence. The solid curve represents the distribution of particles with ejection energies between 0 and 1 eV, the dashed curve (---) for energies between 2.5 and 3.5 eV, the dotted curve (·····) the one with energies between 5.0 and 7.0 eV, the dot-dashed curve (-·-·) the one with energies between 7.0 and 9.0 eV, the two-dot-dashed curve (-··-··) the one with energies between 10.0 and 13.0 eV, and the three-dot-dashed curve (-···-···) the one with energies between 13.0 and 16.0 eV.

small particle energies (0 - 1 eV) is governed by the atomic arrangement of only the top two surface layers. Angle-resolved secondary particle mass spectrometry can thus be extremely sensitive to the surface for analysis of material properties when it is operated at small energies.

As the ejection energy was increased, the sputtering intensity in the <2$\bar{1}\bar{1}$> direction increased to a maximum. The ratio of the sputtering intensity in the <$\bar{2}$11> direction to that in <2$\bar{1}\bar{1}$> varied with the ejection energy, although the intensity at <$\bar{2}$11> was consistently greater than that at <2$\bar{1}\bar{1}$>. The observed equal intensities along the directions with $\phi = 30^\circ$ and $\phi = 90^\circ$ in Fig. 2 may thus result from the contribution to the intensity from other polar angles of ejection. The sputtering intensity at <$\bar{2}$11> is related to the ejection of atoms in the direction of the close-packed row of atoms extending in the bulk along the <211> azimuth, whereas the intensity at <2$\bar{1}\bar{1}$> is related to that in the direction of the non-close-packed row of atoms.

The effect of the ejection energy on the angular distribution was further examined for particles sputtered with large kinetic energies. Predictions based on the present sputtering theory failed in analysis of surface bonding structures when particles of energy more than 30 eV were detected. Details of the azimuthal angle distributions at various polar angles of ejection are presented in the form of the spot pattern. The pattern shown in Fig. 4 was made by placing an imaginary flat-plate detector at an arbitrary distance above the crystal surface. Each spot represents the intercept position in the plate detector of the momentum vector of an individual ejecting particle. The center of the plot corresponds to ejection of a particle along a direction normal to the surface. The radial distance of the spot is proportional to tanθ, θ being the polar angle of ejection measured from the surface normal. The vertical direction is related to the <211> azimuth of the fcc {111} face, with the positive direction corresponding to <$\bar{2}$11> and the negative direction <2$\bar{1}\bar{1}$>. The horizontal direction corresponds to the <110> azimuth. The azimuthal angle distribution is extremely sensitive to variations in the ejection energy in the regime of large energy. Although large densities of spots in all plots in Fig. 4 were invariably observed along the <2$\bar{1}\bar{1}$> and <$\bar{2}$11> azimuths, significant variation of the sputtering intensity were found for ejection along these two directions. The relative sputtering intensity between <2$\bar{1}\bar{1}$> and <$\bar{2}$11> azimuths altered greatly as the ejection energy increased. At energies between 45 and 55 eV the sputter intensity at <$\bar{2}$11> exceeded that at <2$\bar{1}\bar{1}$>. However, the intensity increased more along <2$\bar{1}\bar{1}$> than along <$\bar{2}$11> for particles ejected with energies between 60 and 75 eV. Further increased detection energy between 250 and 500 eV resulted in the relative sputtering intensity between the two <211> azimuths becoming reversed again. This feature of alternating relative sputtering intensities at increasing energies would not be readily observable if calculations of only a few hundred trajectories were performed.

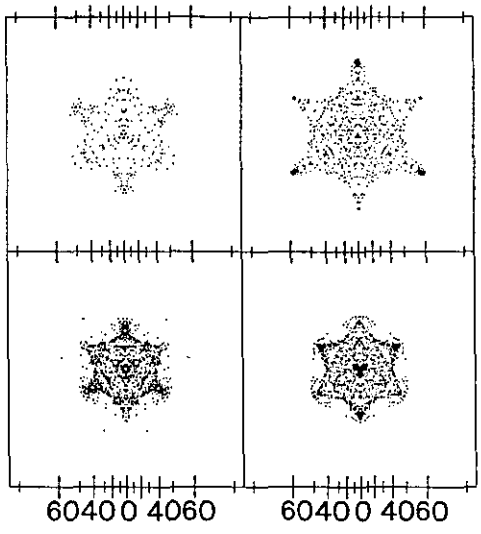

Fig. 4. Spot pattern of particles ejected with kinetic energies of 45 - 55 eV (lower left), 60 - 75 eV (lower right), 115 - 125 (upper left), and 250 - 500 eV (upper right) from the Ag{111} surface under bombardment by normally incident Ar atoms with energy 2 keV. Each spot represents an ejected atom and is plotted at a radius of tanθ, θ being the polar angle of ejection, as for a flat plate collector. The numbers on the abscissa refer to the polar deflection angle given in degrees. The horizontal direction corresponds to the <110> azimuth of the {111} face and the vertical one the <211> azimuth.

The alternating relative sputtering intensity (Fig. 4) cannot be readily explained based on the present theoretical model, which indicates that energetic particles are sputtered along open channels at the surface. To understand better this alternation of sputtering intensities along two major open channels on the surface requires closer examination of the ejection process. Detailed mechanistic information about the collision-induced particle sputtering process may then be extracted by tracing individual collision cascades initiated by incident particles. Results of mechanistic studies of the sputtering process that leads to particle ejection from the surface are presented in Figs. 5, 6, and 7. These figures were selected from more than a hundred similar calculations to present best the points to be mentioned below. A time-exposure atom-motion representation of the collision cascade is used in these figures to exhibit in detail the development in time of the atomic displacement sequence in three dimen-

sions in the solid surface. Cascade analysis of the ejection mechanism according to this pictorial approach reveals that ejection of particles with varied energies and to various angles is due to diverse individual sputtering processes. The most common mechanism is associated with a skip hit of the sputtered atom by its nearest neighbor, shown in Fig. 5. Here the trajectory of the primary particle is depicted by a series of symbols, with the plus (+) representing the particle motion above the top surface layer, the cross (×) the motion between the first and second atomic layers, the upright triangle (Δ) the motion between the second and third layers, the downward triangle (▽) the motion between the third and fourth layers, and the square (□) the motion below the fourth layer. The size of the symbol represents the vertical height of the primary particle within the designated space. The smaller is the symbol, the more deeply the particle moves into the crystal. Furthermore, the scattering path of each substrate atom is portrayed by a string of circles and the interval between two successive circles was arbitrarily chosen to be ten calculation timesteps. The first-layer atoms are marked by open circles. The size of the circle depicts the vertical displacement of the atom in the substrate, with the smaller one representing an atom being displaced more deeply into the substrate. The heaviness of the circle is used to indicate the sequence of the atomic movement in time, with lighter ones representing the atom in earlier timesteps of the collision cascade.

As shown in Fig. 5, the primary particle struck the target atom and then moved down into the bulk of the crystal. The target atom was thus driven to move in the direction with $\phi \sim 150°$ and into the space between the first and second layers of the substrate. On its way moving down into the crystal, the target atom hit on the side its nearest neighbors in the first layer and caused one neighboring atom to move upward and to eject from the surface along the direction with $\phi \sim 90°$ and with a kinetic energy 0.8 eV. Another first-layer neighbor was also caused to eject along the direction with $\phi \sim 210°$ and with a kinetic energy 12.5 eV. In general, an ejection process of this type occurred when a first-layer atom collided with a nearest neighbor in the same layer or a nearest or third-nearest neighbor in the second atomic layer. The ejected atoms from the skip-hit process generally had small kinetic energies.

Atomic ejection from the {111} face of the face-centered-cubic crystal may also be caused by collisions between atoms that are aligned near the direction of ejection. An ejection process of this type is illustrated in Fig. 6, in which the second-layer atoms are represented by dotted circles. The primary atom impinged on the surface and penetrated rapidly into the space between the second and third atomic layers before reflecting upwards. Upon reflecting from the third atomic layer, it forced an atom in the second layer to move upwards along the direction of a non-close-packed row of atoms in the substrate. The atom from the second layer then traveled along the atomic row and pushed from behind an atom in the first layer. The latter atom thus moved upwards and ejected from the surface with a kinetic

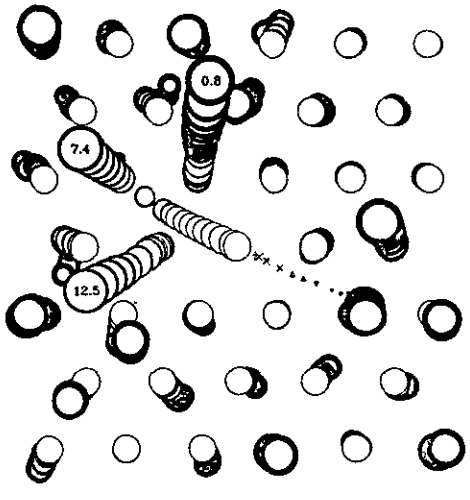

Fig. 5. Atom-motion picture of the collision cascade in three dimensions in time. Shown here are only atomic displacement sequences near the point of primary impact in the first layer of the Ag{111} surface under bombardment by normally incident Ar atoms of energy 2 keV.

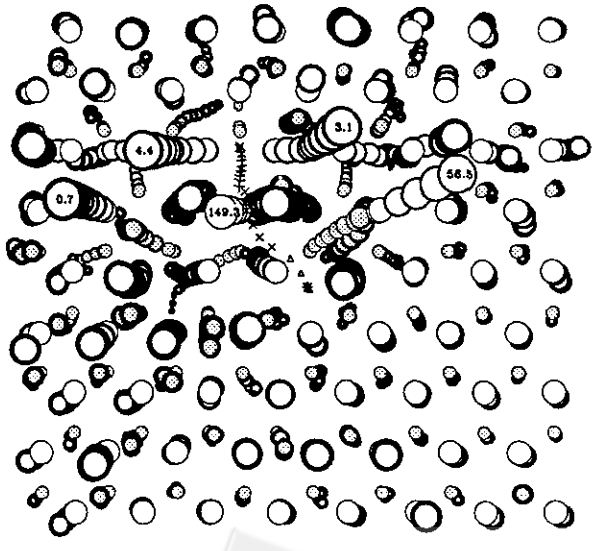

Fig. 6. Atom-motion picture of the collision cascade in three dimensions in time. Shown here are only atomic displacement sequences near the point of primary impact in the top two layers of the Ag{111} surface under bombardment by normally incident Ar atoms of energy 2 keV.

energy 56.5 eV. A similar ejection mechanism caused another atom of the first layer to emit from the surface with a kinetic energy 0.7 eV. Also shown in the figure are atoms ejected by means of the skip-hit mechanism with the primary particle that was backscattered from the third atomic layer of the crystal. As the primary particle was scattered to the space between the first and second layers, it forced an atom of the first layer to eject with a kinetic energy 149.3 eV. Another two atoms of the first layer along the scattering trajectory of the primary particle were struck glancing blows and caused to eject with kinetic energies 4.4 eV and 3.1 eV, respectively.

The momentum transferred from the incident particle may also be retained in an atomic plane perpendicular to the surface for a large distance before resulting in emission of substrate atoms. Presented in Fig. 7 is a cascade developed with the momentum retained in a plane perpendicular to the surface along a <211> direction. The primary particle struck the surface and moved rapidly to the space between the second and third layers before being backscattered. As it left the surface with a kinetic energy 80.6 eV, it knocked

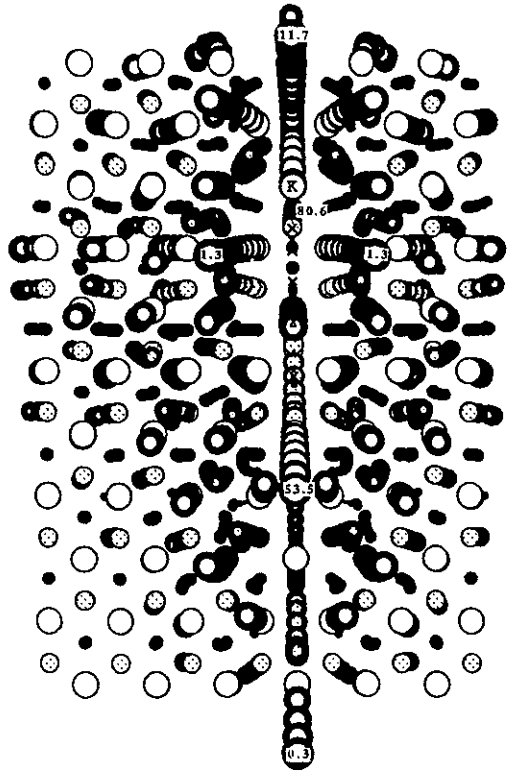

Fig. 7. Atom-motion picture of the collision cascade in three dimensions in time. Shown here are only atomic displacement sequences near the point of primary impact in the top three layers of the Ag{111} surface under bombardment by normally incident Ar atoms of energy 2 keV.

the first-layer atom K downwards. The atom K in turn pushed its neighboring atom in the first layer in the perpendicular plane along the <211> direction to eject with a kinetic energy 11.7 eV. The momentum of the primary particle was also retained in the plane and caused ejection of particles with kinetic energies 53.5 eV and 0.3 eV, respectively. This ejection process bears some resemblance to the alternating mechanism reported for momentum being transmitted through the close-packed string of atoms in the first layer.[34] Our results show that the momentum is retained in the plane perpendicular to the surface and can be transmitted through both close-packed and non-close-packed rows of atoms in the plane. The transmission distance may be even more than 2 nm from the point of primary impact.

The presence of unique sputtering processes for particles ejected at varied angles and with various energies thus resulted in variation with the ejection energy of the angular distribution of particles sputtered from the surface. The variation of the angular distribution with ejection energy may somewhat limit the analytical application of secondary particle mass spectrometry. Without the aid of computer simulations, the technique in its present form may not be employed to determine precisely surface bonding structures, especially when energetic particles are selected for detection. Further tests of the dependence of the angular distribution upon the duration of collision reveal that by collecting particles of selected durations of collision the analytical capability of the technique to characterize atomic bonding geometries on the surface may be significantly improved. In the calculation, the duration of collision is determined as the time (in fs) required for a certain substrate atom to pass the boundary of the interaction potential and to eject from the surface after primary impact. The longer is the collision, the more the ejecting substrate atom is retained in the surface. Shown in Fig. 8 are spot patterns of particles ejected from the surface with varied durations of collision. By selecting only those particles in relatively prolonged collisions the fraction of particles ejecting along preferred crystallographic directions is enhanced considerably. The preferred directions of ejection and the relative sputtering intensity between major open channels vary insignificantly with the duration of collision in the regime 150 - 300 fs. Particles of prolonged collisions leave the surface late in the collision cascade. As mentioned, the surface channel is retained to some extent during sputtering, because the structural damage introduced by the incident particle is localized. Thus, instead of ejecting to a wide angle as in the case of energetic particles, the particles of prolonged collisions are well confined along the open channel between the surface atoms. Their angular distribution thus reflects well the

bonding geometry of the surface.

CONCLUSION

The present sputtering theory was closely examined for precise analysis of the atomic bonding geometry on the surface using secondary particle mass spectrometry. The sputtering process is localized near the point of primary impact in the surface. More than 90% of particles are ejected within four lattice spacings from the target when a Ag{111} surface is bombarded by Ar atoms of energy 2 keV. The ratio of the number of particles sputtered from the top surface layer to the total number of the sputtered particles is about 95%. At small ejection energies (0 - 1 eV), a large variation in the sputter intensities along two major open channels in the surface was observed. Hence in this energy regime the ejection behavior of the sputtered particles is governed by the atomic arrangement of only the top two surface layers. The high sputtering yield from the top surface layers and the unique ejection behavior at small energies render secondary particle mass spectrometry an analysis technique highly sensitive to the surface. As the technique can be sensitive to only the top two surface layers, it may be utilized to explore chemical processes of underlayer adsorption, such as oxygen on metal surfaces,[35,36] and subsurface growth, such as the initial growth of metal silicides in silicon,[37] in great detail.

The ratio of the sputtering intensity along the direction $<\bar{2}11>$ to that along $<2\bar{1}\bar{1}>$ varies significantly with the ejection energy in the regime of large energy. Ejection of particles at varied angles and with varied energies resulted from varied individual collision cascades. The energetic particles ejected at a wide angle and their paths may not be confined along directions of open spacings between surface atoms. However, the preferred directions of ejection and the relative sputtering intensity between major open channels vary insignificantly with the duration of collision for prolonged collisions. More angle-resolved structure in the angular distribution may thus be obtained for better analysis of bonding geometries on surfaces when particles from prolonged collisions, rather than particles with large energies, are detected.

The energy distribution of ejected particles in the energy regime beyond the maximum energy decayed as $1/E^n$; E is the ejection energy and n about 0.8 for particles sputtered along the direction with $\phi = 30^\circ$ and about 1.2 for those along the direction with $\phi = 90^\circ$. It is also desirable to characterize the energy distributions at specific angles of ejection so as to characterize better the sputtering process. Knowledge of the energy distribution of the sputtered species is also important for the development of the quantitative secondary particle mass spectrometric method,[38] for the determination of variation of work function,[39] for the analysis of the chemical state of surface atoms,[40] and for the improvement of the device performance.[41,42] Further investigation of the energy distribution is in progress.

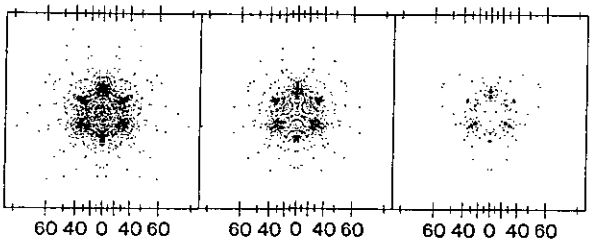

Fig. 8. Angular distribution of particles ejected with kinetic energies 7 - 9 eV and with all collision durations (left), with collision durations greater than 150 fs (middle), or with collision durations greater than 200 fs (right) from the Ag{111} surface under bombardment by normally incident Ar atoms of energy 2 keV. See Fig. 4 and the text for other details.

ACKNOWLEDGMENT

I thank the National Science Council of the Republic of China for support.

Received March 26, 1994.

Key Words

Secondary particle mass spectrometry; Surface analysis; Sputtering theory; Molecular dynamics.

REFERENCES

1. Smith, H. I.; Craighead, H. G. *Phys. Today* **1990**, *February*, 24.
2. Kern, D. P.; Kuech, T. F.; Oprysko, M. M.; Wagner, A.; Eastman, D. E. *Science* **1988**, *241*, 936.
3. Woodruff, D. P.; Delchar, T. A. *Modern Techniques of Surface Science*; Cambridge University Press: Cambridge, **1986**.
4. Benninghoven, A.; Rudenauer, F. G.; Werner, H. W. *Secondary Ion Mass Spectrometry*; John-Wiley: New York, **1987**.
5. Oechsner, H. In *Thin Film and Depth Profile Analysis*,

Oechsner, H. Springer-Verlag: Berlin Ed.; **1984**, 63.
6. Anderson, G. S.; Wehner, G. K. *J. Appl. Phys.* **1960**, *31*, 2305.
7. Winograd, N.; Garrison, B. J.; Harrison, D. E., Jr. *Phys. Rev. Lett.* **1978**, *41*, 1120.
8. Holland, S. P.; Garrison, B. J.; Winograd, N. *Phys. Rev. Lett.* **1979**, *43*, 220.
9. Winograd, N.; Garrison, B. J.; Harrison, D. E., Jr. *J. Chem. Phys.* **1980**, *73*, 3473.
10. Kapur, S.; Garrison, B. J. *J. Chem. Phys.* **1981**, *75*, 445.
11. Gibbs, R. A.; Holland, S. P.; Foley, K. E.; Garrison, B. J.; Winograd, N. *J. Chem. Phys.* **1982**, *76*, 684.
12. Kobrin, P. H.; Schick, G. A.; Baxter, J. P.; Winograd, N. *Rev. Sci. Instrum.* **1986**, *57*, 1354.
13. Gibbs, R. A.; Winograd, N. *Rev. Sci. Instru.* **1981**, *52*, 1148.
14. Baxter, J. P.; Singh, G. A.; Singh, J.; Kobrin, P. H.; Winograd, N. *J. Vac. Sci. Technol.* **1986**, *4*, 1218.
15. Chang, C.-C.; Winograd, N. *Surface Sci.* **1990**, *230*, 27.
16. Chang, C.-C. *Mat. Res. Soc.* **1992**, *278*, 287.
17. Harrison, D. E. *Radiation Eff.* **1983**, *70*, 1.
18. (a) Harrison,D. E., Jr. *Crit. Rev. Sol. St. Mater. Sci.* **1988**, *14*, S1; (b) Harrison, D. E., Jr.; Kelly, P. W.; Garrison, B. J.; Winograd, N.; *Surface Sci.* **1978**, 76, 311; (c) Chang, C.-C. *Surface Interface Anal.* **1990**, *15*, 79.
19. Firsov, O. B. *JETP (Sov. Phys.)* **1958**, *6*, 534.
20. Chang, C.-C. *Phys. Rev.* **1993**, *B48*, 12399.
21. Jackson, D. P. *Radiation Eff.* **1973**, *18*, 185.
22. Chang, C.-C. *Formosan Sci.* **1993**, *46*, 9.
23. Chang, C.-C. unpublished results.
24. Deline, V.; Evans, C. A. Jr.; Williams, P. *Appl. Phys. Lett.* **1978**, *33*, 578.
25. Chang, C.-C.; Lung, C.-H. *Chem. Phys. Lett.* submitted.
26. Thompson, M. W. *Philos. Mag.* **1968**, *18*, 377.
27. Sigmund, P. *Phys. Rev.* **1969**, *184*, 383.
28. Sigmund, P.; Oliva, A.; Falcone, G. *Nucl. Instr. Methods* **1982**, *194*, 541.
29. Yamamura, Y. *Nucl. Instr. Methods* **1982**, *194*, 515.
30. Garrison, B. J. *Nucl. Instr. Methods* **1986**, *B17*, 305.
31. Thompson, M. W. *Phil. Mag.* **1968**, *18*, 377.
32. Winograd, N.; Baxter, J. P.; Kimock, F. M. *Chem. Phys. Lett.* **1982**, *88*, 581.
33. Thompson, D. A. *Radiation Eff.* **1981**, *56*, 105.
34. Harrison, D. E., Jr.; Delaplain, C. B. *J. Appl. Phys.* **1976**, *47*, 2252.
35. Strong, R. L.; Erskine, J. L. *J. Vac. Sci. Technol.* **1985**, *A3*, 1428.
36. Arabczyk, W.; Rausche, E.; Storbeck, F. *Surface Sci.* **1991**, *247*, 264.
37. Luo, L.; Smith, G. A.; Hashimoto, S.; Gibson, W. M. *Surface Sci.* **1991**, *249*, L338.
38. Deng, R.-C.; Williams, P. *Anal. Chem.* **1989**, *61*, 1946.
39. Wittmaak, K. *Phys. Scr.* **1983**, *T6*, 71.
40. Solomon, J. S. *J. Vac. Sci. Technol.* **1988**, *A6*, 81.
41. Ohwaki, T.; Taga, Y. *Appl. Phys. Lett.* **1989**, *55*, 837.
42. Takagi, T. *Thin Solid Films* **1982**, *92*, 1.